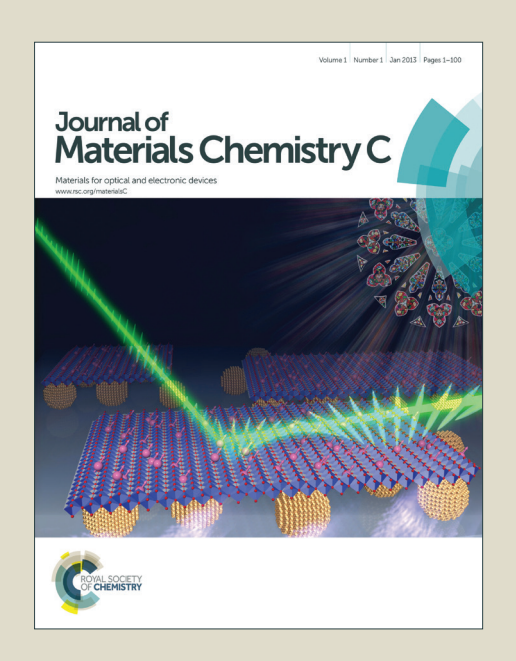
Journal of Materials Chemistry C

Accepted Manuscript



This is an *Accepted Manuscript*, which has been through the Royal Society of Chemistry peer review process and has been accepted for publication.

Accepted Manuscripts are published online shortly after acceptance, before technical editing, formatting and proof reading. Using this free service, authors can make their results available to the community, in citable form, before we publish the edited article. We will replace this Accepted Manuscript with the edited and formatted Advance Article as soon as it is available.

You can find more information about *Accepted Manuscripts* in the **Information for Authors**.

Please note that technical editing may introduce minor changes to the text and/or graphics, which may alter content. The journal's standard <u>Terms & Conditions</u> and the <u>Ethical guidelines</u> still apply. In no event shall the Royal Society of Chemistry be held responsible for any errors or omissions in this *Accepted Manuscript* or any consequences arising from the use of any information it contains.



Materials Chemistry C

Cite this: DOI: 10.1039/c0xx00000x

PAPER www.rsc.org/xxxxxx

Enhanced conductivity and photoresponse in rubrene singlecrystal/PCBM film interface†

Rui M. Pinto, a,b Ermelinda M. S: Maçôas and Helena Alves*

Received (in XXX, XXX) Xth XXXXXXXXX 20XX, Accepted Xth XXXXXXXX 20XX 5 DOI: 10.1039/b000000x

A large photoresponse is observed at the interface between a highly ordered rubrene single-crystal and an amorphous fullerene film, with responsivity values 300 times higher than the corresponding bulkheterojunctions and isolated single-crystal. The rubrene: PCBM interface displays a wide range photoresponse, particularly enhanced in the red part of the visible spectrum presenting an exceptionally 10 high photogeneration yield for lower excitation energies. Increased dark conductivity and electronic structure calculations indicate a polarization effect that reduces the band-gap and assists interfacial excitons separation to donor and acceptor layers well apart, minimizing electron-hole recombination. Wavelength-dependent photoconductivity and thickness-dependent absorption measurements, supported by computational analysis, show that primary excitons formed in rubrene and PCBM evolve to excitons 15 which are effectively separated at the interface. Our results provide important insights to harnessing excitons generated in both the electron donor and acceptor materials increasing the efficiency in organic devices.

Introduction

Small conjugated molecules have been investigated due to their 20 high absorption coefficient and ordered molecular arrangements, giving rise to the generation of delocalized excited states and promotion of intermolecular charge transport, determinant factors for efficient optoelectronic devices such as field-effect transistors^{1,2} and photovoltaic cells.^{3,4} Several strategies have 25 been envisioned to improve efficiency in excitonic devices, such as chemical modifications to achieve a more appropriate spectral range, regulating the thickness and organization of the active layers⁵ or using multilayer semiconductors with different spectral coverage. Diligence has focus mostly on the donor layer, and the 30 role of the acceptor has been reduced to the promotion of charge separation and conduction, with ensuing collection. However, an increased efficiency can be anticipated if excitons generated in both the acceptor and donor layers can be collected. Among the factors that lead to difficulties in promoting exciton generation in 35 acceptors is the usually low absorption in the visible region exhibited by the most popular acceptors in excitonic solar cells. This is the case of the most widely used acceptor in bulk heterojunction (BHJ) solar cells, [6,6]-phenyl-C₆₁-butyric acid methyl ester (PCBM), absorbing mostly below 400 nm.8 Some 40 small molecule acceptors present enhanced light absorption in the visible region, such as the perylenes or the perfluorinated subphthalocyanines, 9,10 but the performance in solution processed BHJ remains rather poor and even flat heterojunctions are less efficient than fullerene based devices. The existence of 45 morphology constriction with interfacial disorder is one of the

acceptor in BHJs. Strongly anisotropic electron mobility in π stacked arrangements in the solid phase has also been pointed out as limiting efficient charge collection. Recently, the use of 50 crystalline materials in organic interfaces has presented high photoresponse, and enabled a better understanding of the morphology role in exciton diffusion and separation.¹¹

Herein, we investigate the photocurrent generation in the visible region of an organic interface composed of an amorphous 55 PCBM film and a highly ordered rubrene single-crystal (SC). In this interface, the ease of solution processing organic films is combined with the improved charge-transport and long exciton diffusion length of single-crystals. 12,13 We show that such interfaces present responsivity values 300 times higher than 60 rubrene 14 or PCBM:rubrene films, through the entire visible region, with a particularly high efficiency in the 500-800 nm range, where absorption is extremely weak. Such enhanced response is interpreted as an efficient contribution of excitons generated on both the donor and acceptor materials and discussed 65 in terms of electronic structure calculations.

Experimental section

Interface preparation

Rubrene and PCBM (Sigma-Aldrich) were used as source materials, and HPLC chlorobenzene (Sigma-Aldrich) as solvent. 70 Rubrene single-crystals were grown at ~310 °C by physical vapour transport, under a stream of argon. Thoroughly cleaned glass was used as substrate. PCBM film (~500 nm thick) was obtained by spin-coating (100 rpm/ 5 s + 1500 rpm/ 30 s) a filtered PCBM:C₆H₅Cl (10 mg mL⁻¹) solution. Thicker films of

factors that could explain the poor performance of molecular

PCBM were formed by drop-casting this solution onto glass substrates. The interfaces were assembled by laminating thin rubrene single-crystals (200-800 nm thick) on top of the PCBM films, while using carbon paste as contacts. Crystal and film 5 thicknesses were determined using a Dektak 3030ST profilometer. The lamination technique is successfully used on single-crystal field effect transistors^{12,15} or in charge transfer interfaces¹⁶ (Fig. 1). Such approach circumvents interfacial structural disorder and phenomena such as chemical recombination or interdiffusion, usually associated with solution or vapour layer processing, and potentially leading to interfaces with unique electronic characteristics. ^{16,17} Samples of rubrene single-crystals and PCBM films were also prepared for comparison.

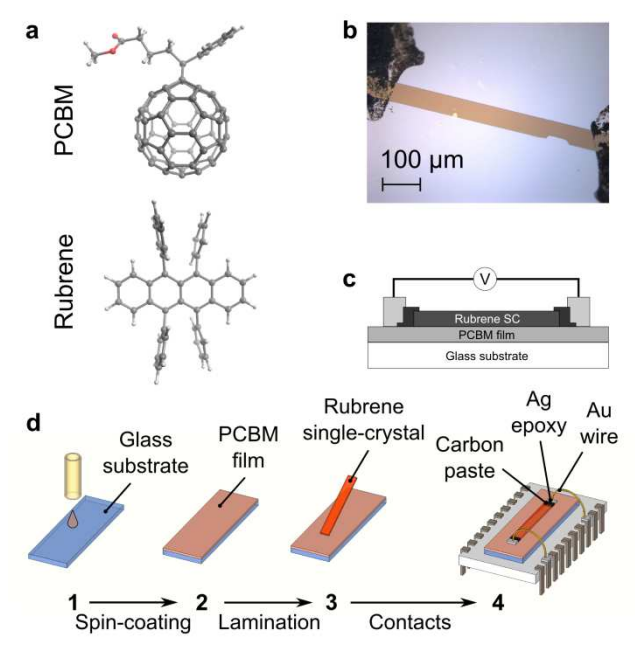


Fig. 1 (a) Molecular structure of PCBM and rubrene. (b) Image of a PCBM/rubrene interface with carbon contacts. (c) Cut-view illustration of the interface. (d) Process of interface assembly: spin-coating (1-2), crystal lamination (3) and wire-bonding (4).

${\scriptstyle 20}$ Absorption and photocurrent measurements

UV-vis absorption spectra were obtained using a Jasco V-660 UV-vis double beam spectrophotometer. I-V characteristics were taken with a Keithley 237 source-measure unit. Interface dimensions were W=10-700 μm and L=300-1500 μm, with W/L~0.4. For photocurrent measurements, a system comprised of a 250 W quartz tungsten halogen lamp, monochromator, a Thorlabs S121C Si photodiode and a longpass filter with a 550 nm cut-on wavelength was used. Samples (w/ contacts) were irradiated at normal incidence using non-polarized light, through the (a,b) facet of rubrene crystals (top illumination). Absorbance of rubrene SC was measured using the same geometry and it was not corrected for reflectivity. All measurements were performed in air, under ambient conditions.

35 Computational details

All computations were performed with GAMESS, 18 using

Hartree-Fock and density functional theory (DFT) methods. B3LYP and CAM-B3LYP were used with the 6-31G basis set. The system was modelled within the frozen monomer 40 approximation, after optimization (CAM-B3LYP/6-31G) of the individual molecules (rubrene C2h, PCBM C1), including Grimme's dispersion corrections. The dimer geometry was not optimized. Singlet excitation spectra were computed in the timedependent DFT framework, using B3LYP and CAM-B3LYP. 45 Simulated absorption profiles were obtained by dressing excitation energies with Lorentz functions (fwhm=0.25 eV), scaled to the transition strengths. Such broadening mimics the experimental resolution in our photoresponse measurements. Electronic couplings were computed using the projective 50 method. 19 We note that the calculations on the heterodimer provide an incomplete description of the energetic of the interface, due to the reduced size of the model and the limited donor-acceptor orientations analyzed. In a realistic interface, medium polarization and nanomorphology constraints strongly 55 affect the conduction and valence levels of donor and acceptor materials, and the energetics at the interface.

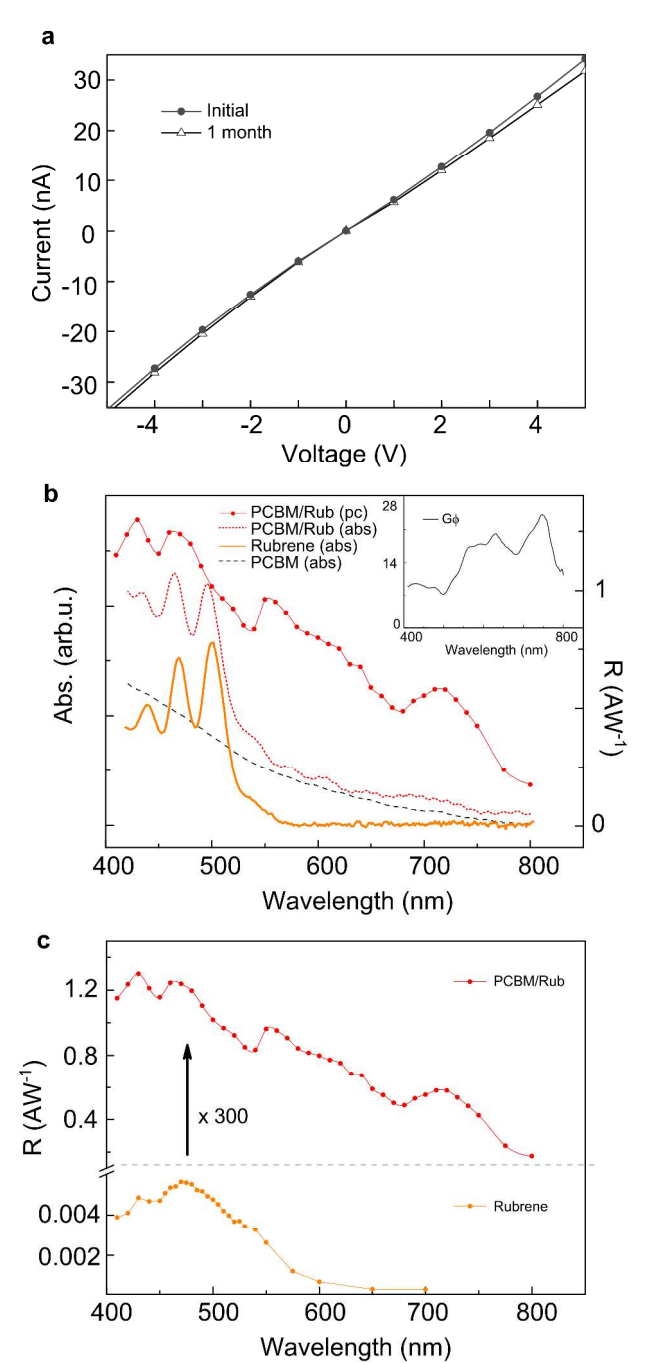
Results and discussion

Conductivity measurements on the PCBM/rubrene interface (using sub-µm thick crystals) were performed to analyze the 60 interfacial electrical behaviour. The I-V characteristic is presented in Fig. 2a. The long channel (500-1500 µm) ensures that charge injection is not contact limited, reflecting directly the properties of the interface constituent materials. In Fig. 2a, two I-V curves obtained from the same sample stored in air for almost 65 one month, show that interfaces maintain their electric properties over time. The sheet resistance R_{sqr} of the interfaces ranges 10-50 $M\Omega$, from a sampling universe of ca. 50 devices (see ESI, Fig. S1), in contrast with tenths of $G\Omega$ measured in rubrene SCs. The PCBM film alone does not show any measurable conductivity in 70 the same experimental conditions. This low resistivity generated at the interface between electron donor and acceptor materials with very different electrical performance is also observed in charge-transfer interfaces between two single-crystals. 16,17 The high density of charge observed was understood in terms of a 75 charge-transfer process promoted by an interfacial bandbending.16

The absorption spectra of the interface and its components are shown in Fig. 2b. In PCBM, the spectrum has a strong absorption in the near-UV with a weak absorption tail extending into the 80 visible and near-IR, as previously observed. 20 This broad and unstructured absorption tail, shown in Fig. 2b, has contributions from different transitions. These include the highest occupied molecular orbital (HOMO) to lowest unoccupied molecular orbital (LUMO) transition centred on the C₆₀ cage, which has 85 been observed at ~ 700 nm. 14,20,21,22 The absorption spectrum of single-crystal rubrene is in agreement with earlier reports, 11,13,23 showing a pronounced vibrational progression, with the 0-0 transition appearing as a shoulder at 534 nm and the strongest vibronic band peaking at 495 nm. PCBM-rubrene interface 90 follows the spectral profile of its isolated components, being well described by the superposition of the absorption spectra of PCBM film and rubrene single-crystal.

The photocurrent excitation spectrum (λ = 400-800 nm) of the

interface is compared with that of rubrene SC in Fig. 2c, showing an enhanced photocurrent in PCBM/rubrene interface. Figs. 2b and 2c illustrate three central observations of this work. First, the



5 Fig. 2 (a) I-V characteristics of a PCBM/rubrene interface, showing no signs of degradation after one month storage under ambient conditions.
 (b) Comparison between the photocurrent spectra of PCBM/rubrene interfaces and absorption spectra of PCBM film (~500 nm thick), rubrene SC (~400 nm thick) and PCBM/rubrene interface. The low amplitude oscillations in the interface absorption spectrum are due to interference effects within rubrene SC. The inset in the upper panel shows the photocurrent yield, G·Φ. (c) Spectral responsivity of rubrene SC and PCBM/rubrene interface.

responsivity of PCBM/rubrene interface (1.2 A/W) is 2-3 orders of magnitude higher than rubrene (4 mA/W). This not only

represents an improvement over the photoconductivity of rubrene, but it is also a remarkable improvement over PCBM:rubrene BHJ systems, with a responsivity of only 4.3 mA/W.²⁴ Second, the presence of PCBM extends the photoconductivity into the 600-800 nm region. This is clearly noticed on the photocurrent excitation spectrum of the interface where the responsivity between 600-800 nm is highly amplified when compared with the responsivity of rubrene (Fig. 2c). Finally, the absorption spectrum of the interface differs from the corresponding photocurrent excitation spectrum (Fig. 2b), with a clear reduction of at least one order of magnitude between absorption at 600-800 nm vs. 400-600 nm, whereas the photoresponse only diminishes by a factor of 2.

Since, by definition, the photocurrent yield is the number of charges collected per absorbed photon (n_e/n_p) , it can be expressed by the product $G \cdot \Phi$ of the internal photogeneration quantum efficiency Φ (known as the IQE) and the gain G. The measured responsivity $(R = I_{pc}/P_{exc})$ gives an estimative of the yield:

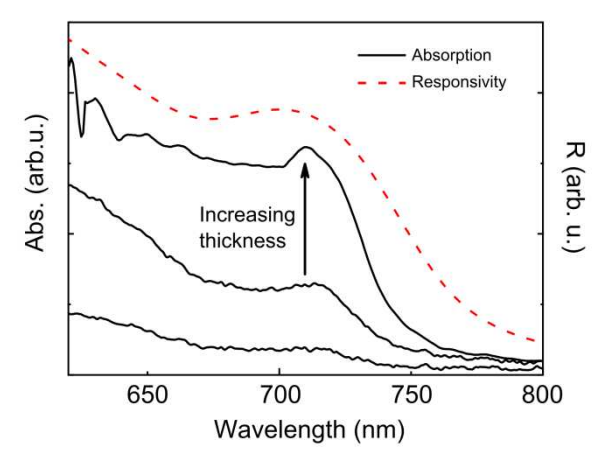
$$\textbf{G} \cdot \boldsymbol{\Phi} = n_{\textbf{g}}/n_{\textbf{p}} = \frac{I_{\textbf{p}\textbf{c}}/e}{(F_{\textbf{c}\textbf{c}\textbf{c}}/hv)\cdot (1 \cdot 10^{\text{vA}})} = \frac{hcR}{e\lambda (1 \cdot 10^{\text{vA}})} \tag{1}$$

35 where I_{pc} is the photocurrent, P_{exc} is the excitation power and 1-10^{-A} gives the fraction of absorbed photons (wherein A is the absorbance). The third central observation, and perhaps the most remarkable one, corresponds to a higher photocurrent yield for excitation at lower energies (see inset in Fig. 2b). Since, rubrene 40 is virtually transparent in the 600-800 nm region, and there is no correlation between the shape of the interface photoconductivity spectra and the thickness of the different rubrene crystals probed (see ESI, Fig. S6), the observed photoconductivity is either due to excitons generated in PCBM or direct excitation of ground-state 45 CT states. Another observation in the 700-750 nm region is the photocurrent yield reaching a maximum value superior to unit, which indicates the existence of a photomultiplication mechanism. Photoconductivity gain has also been reported in polycrystalline organic composite films of rubrene and 9,10-50 diphenylanthracene, 14 in pentacene films deposited onto coplanar interdigitated-electrode structures, 25 in several polymer based diodes, 26 and in highly ordered crystalline interfaces of TCNQ and rubrene. 11 Different factors can lead to a photocurrent gain, such as differences between charge mobility and charge 55 accumulation at the contacts. Such gain is deeply connected with the lifetime of the charge separation state, which is independent on the nature of the primary excitons. Thus, the spectral dependence of the photogeneration yield must originate from the charge generation quantum yield.

The absorption and photocurrent spectra can provide indications to where the excitons are originally formed. These can be formed in the donor layer, in the acceptor or through direct excitation of a charge transfer state belonging to an interfacial van der Waals complex. In the 400-600 nm range, the interface photocurrent generation spectrum matches that of an isolated rubrene single crystal (Fig. 2c), and the high responsivity values of the PCBM:rubrene interface are similar to those of the TCNQ:rubrene interface. Both observations support an important contribution of excitons localized in rubrene to the photoconductivity in the 400-600 nm region. In the 600-800 nm,

where the photocurrent yield is higher, the long absorption tail of PCBM extending to the near-IR suggests the photocurrent arises from PCBM excitons. Although not evident in thin films, Fig. 3 shows that in thick PCBM films a $S_0 \rightarrow S_1$ transition is observed 5 at ~720 nm, which is coincident with the lowest energy band in interface photocurrent excitation spectrum. These observations and the absence of new bands in the interface absorption/photocurrent spectra argue against the existence of an interfacial complex with accessible states for direct CT exciton 10 formation. Moreover, attempts to obtain a rubrene-PCBM charge transfer complex in solution were unsuccessful, even when assisted by I₂. However, such complex cannot be ruled out solely on the basis of the absorption spectra since the interfacial volume is rather small (on the monolayer scale). Indeed, direct excitation 15 to an intermolecular CT state was previously observed in PCBM:rubrene blends.²⁴ The responsivity of such blends extends into the 750-850 nm region, whereas in our interfaces the responsivity edge appears at shorter wavelengths and follows the absorption edge of a film of PCBM alone (see Fig. 3).

To shed light on the nature of primary excitons, timedependent DFT was used to model the excited states of the interface by computing the absorption spectrum of an interfacial complex.



 25 Fig. 3 Comparison between responsivity of a PCBM/rubrene interface and absorption of PCBM films (spin and drop-cast) with increasing thickness (0.5-100 μ m) showing the S0 \rightarrow S1 band at \sim 720 nm. Below 620 nm the absorption is saturated.

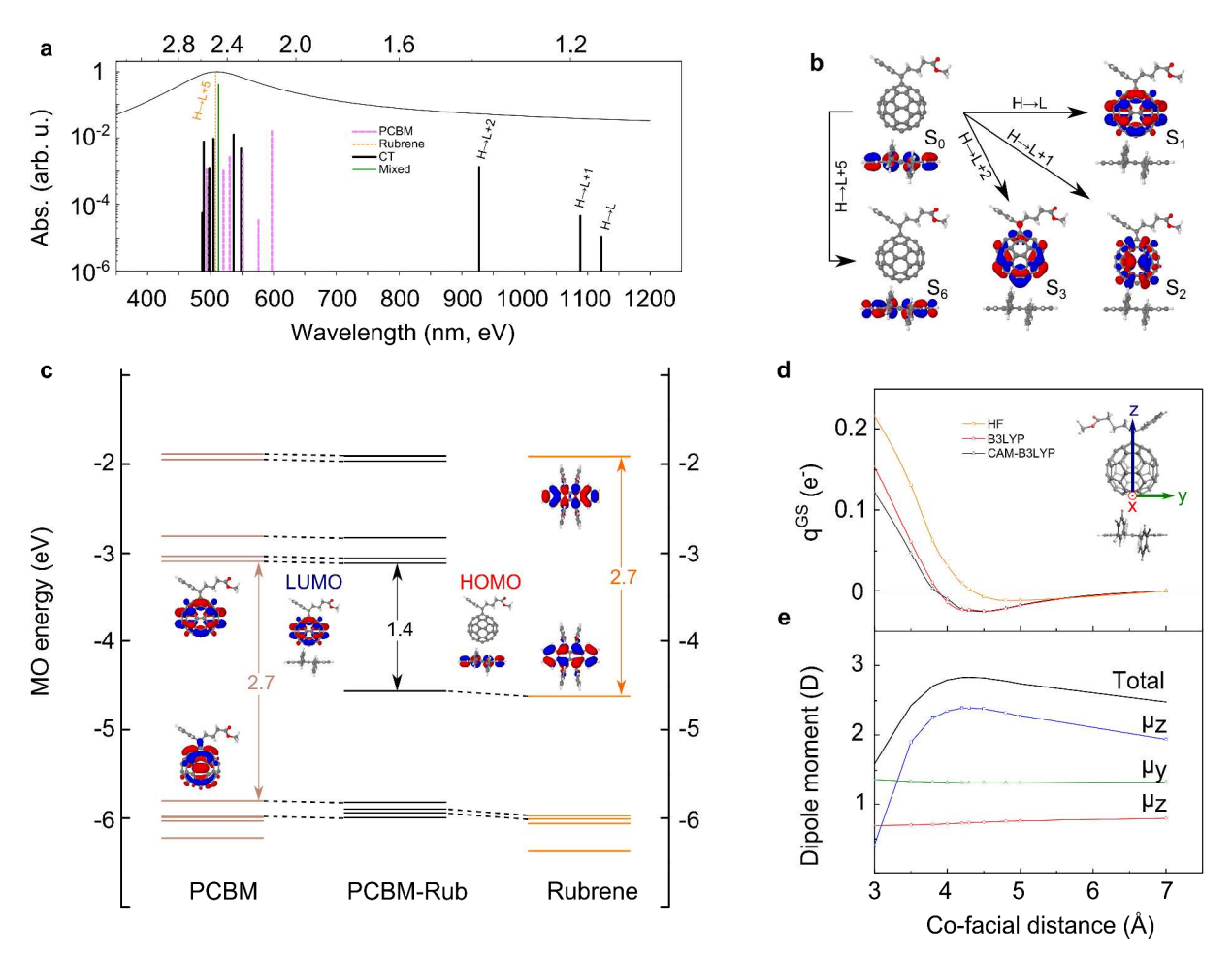


Fig. 4 (a) Absorption stick spectrum of the interface, showing the degree of delocalization of singlet excitations. (b) Iso-contours (0.02) of the MOs involved in the low-lying CT states and rubrene exciton formation. (c) MO energy diagram and frontier orbitals of PCBM, rubrene and PCBM-rubrene (at z=4.2 Å), from B3LYP/6-31G results. (d) Amount of negative charge q^{GS} on PCBM, obtained from Mulliken population analysis. (e) Dipole moment analysis of PCBM-rubrene, from CAM-B3LYP/6-31G results.

Materials Chemistry C

Cite this: DOI: 10.1039/c0xx00000x

PAPER www.rsc.org/xxxxxx

In the theoretical calculations, the geometries of PCBM and rubrene molecules were individually optimized and approximated co-facially, presenting equilibrium distance at 4.2 Å (see ESI, Fig. S2). B3LYP and CAM-B3LYP (Fig. S3) were employed in 5 the computations, but only B3LYP results are presented since they reproduce better the ground-state energy levels, electronic bandgap (Table S1, ESI) and absorption spectra of the isolated components. Even though CAM-B3LYP has been devised to remedy B3LYP poor description of intermolecular excitations, its 10 description of the ground-state levels (HOMO and LUMO), which serve as base for TD-DFT calculations, detracts from known experimental values (see Fig. S7, ESI, for a functional pre-screening based on PCBM).

Fig. 4a shows the simulated absorption spectra at the 15 equilibrium distance and the electronic transitions on the singlet manifold of the interfacial complex, discriminating the degree of delocalization of the transitions. The most relevant MOs of the interfacial complex are displayed in Fig. 4b. The experimental absorption maxima of isolated rubrene (534 nm) and PCBM (331 20 nm) are fairly well predicted by the calculations at 509 nm and 373 nm, respectively. The largest discrepancy lies on the PCBM $S_0 \rightarrow S_1$ transition, which is predicted at 597 nm and observed at 700 nm. This overestimation by 0.3 eV can be partially attributed to differences between the real molecular environment and the 25 theoretical approximation, which considers the molecule in vacuum. Nevertheless, the simulated spectrum clearly indicates that the interface absorbs more strongly in the overlap region of rubrene and PCBM, with an absorption maximum coincident with isolated rubrene (509 nm), corresponding to the generation 30 of an intramolecular rubrene exciton (65%, H→L+5). Around this region, a few low-intensity CT transitions overlap extensively with intramolecular excitations. The strongest of these CT transitions are the H→L+3 (99%) at 537 nm, and the H→L+4 (98%), at 549 nm, with oscillator strengths ~100 times 35 lower than the transition localized on rubrene. Analysis of other contributions to the singlet excitation manifold reveals that the first three low-lying states of an interfacial complex are CT transitions between rubrene and PCBM in the near-IR (Fig. 4a). The MOs involved in these transitions are mainly H→L (99%) at 40 1122 nm, H→L+1 (99%) at 1088 nm, and H→L+2 (99%) at 928 nm (see Fig. 4b). These results support the assignment of the observed photoresponse to excitons that are originally localized on either donor or acceptor components of the interface. Thus, the enhanced photoresponse at 600-800 nm must originate in 45 excitons localized in PCBM, whose weak absorption extends into the NIR. The reason why the lower energy excitons localized in PCBM have higher charge generation yields than the higher energy excitons localized in rubrene remains unclear. In effect, the most common observation in organic D/A blends is that either 50 charge generation yield is unaffected by the excess energy²⁷ or it increases with excitation energy.²⁸ However, it should be noted that different primary excitons lead to distinct separation processes. An oxidative process follows generation of excitons in

rubrene, with the transfer of an electron from the LUMO of 55 rubrene to the LUMO of PCBM, whereas a reductive process is associated to excitons generated in PCBM, leading to the transfer of a hole from the HOMO of PCBM to the HOMO of rubrene.²⁹ In light of the observed higher photogeneration efficiency of PCBM excitons, exciton dissociation rate following hole transfer 60 from PCBM to rubrene is anticipated to be faster than exciton dissociation triggered by electron transfer from rubrene to PCBM. Indeed, the PCBM excitons are very short lived (on the picosecond time scale), and thus the hole transfer process should be an ultrafast process.

The last step of exciton separation into free charge-carriers strongly depends on the interfacial energetics. In Fig. 4c, the molecular orbital (MO) energy diagram of PCBM, rubrene and PCBM/rubrene, is represented using B3LYP results. In this diagram, the complex HOMO and LUMO correspond to orbitals 70 localized on the donor and acceptor molecules, with a slight band gap lowering of ~100 meV (Fig. S4). Another possible factor known to enhance exciton splitting is the formation of an interfacial dipole layer, 30 originated by ground-state chargetransfer³¹ and polarization effects. The analysis of the ground-75 state HOMO-LUMO electronic coupling, the dipole moment, µ, and Mulliken charges helps to understand such effects. Detailed examination revealed that at the equilibrium distance, 4.2 Å, no significant charge is transferred to PCBM (Fig. 4d). In fact, a significant amount of charge, 0.15 e⁻, is only transferred at shorter 80 distances, ~3.0 Å, in agreement with the electronic coupling (Fig. S5). Also, the dipole moment along z decreases as PCBM approaches rubrene (Fig. 4e), implying less positive charge on PCBM due to partial electron transfer from rubrene. Therefore, if a van der Waals complex rubrene-PCBM is formed, it does not 85 seem to present a relevant charge transfer character in the groundstate. Nevertheless, this simple molecular model indicates that mutual polarization takes place in the interfacial region, approximating valence and conduction bands. It is expectable that this polarization effect, together with changer transfer at non-90 equilibrium distances, are responsible for the observed increase of dark conductivity, through formation of an interfacial dipole layer. The charge rearrangement can lead to shifts in relevant energy levels, a band bending on the donor and acceptor molecules at the interface, reducing the band gap. Such band-95 bending is known to take place in other donor-acceptor organic heterostructures, 16.32 and assist the interfacial excitons to overcome their Coulomb attraction, promoting exciton splitting. 11,33 In addition, the charge-transfer interface prepared by crystal lamination separates the generated carriers into the two 100 well defined conductive layers, with holes carried by the HOMO band of rubrene and electrons carried by the LUMO band of PCBM, minimizing electron-hole recombination.

105 Conclusions

Rubrene SCs were laminated on top of PCBM amorphous films, creating a structure with high photoresponse through the entire visible region. The lamination assembly maintains the morphology of each layer, giving rise to an interface with hybrid 5 structural order and a 300-fold increase in photocurrent with respect to rubrene single-crystals or PCBM:rubrene BHJ. Moreover, the photocurrent generation is highly amplified in the wavelength range where absorption is extremely weak, between 500-800 nm. Our results suggest that such response is directly 10 connected to excitons generated on the acceptor. The analysis of the absorption spectra, photoconductivity and electronic structure calculations are consistent with the exciton generation in the bulk of PCBM and rubrene. Polarization effects promote the subsequent charge separation. Our results provide important 15 insights to harnessing excitons generated in both the electron donor and acceptor materials. The increase on the spectral range of the photoresponse and charge generation efficiency promoted by structural order of small molecules and morphologic defined organic interfaces are instrumental for the future design of 20 excitonic devices.

Acknowledgments

The authors thank V. Soares for technical support. The authors acknowledge the Advanced Computing Laboratory at University of Coimbra for providing computing resources. FCT - Fundação para a Ciência e Tecnologia (Portugal) supported this work through financial funding the Associated Laboratory - Institute of Nanoscience and Nanotechnology, project Pest-OE/CTM/LA0024/2011 and grant nr. SFRH/BPD/84820/2012.

Notes and references

- 30 ^a CQFM-Centro de Química-Física Molecular and IN-Institute of Nanoscience and Nanotechnology, Instituto Superior Técnico, 1049-001 Lisboa, Portugal.
- b INESC MN and IN-Institute of Nanoscience and Nanotechnology, Rua
 Alves Redol, 1000-029 Lisboa, Portuga; E-mail: halves@inesc-mn.pt
- 35 † Electronic Supplementary Information (ESI) available. See DOI: 10.1039/b000000x/
 - A. S. Molinari, H. Alves, Z. Chen, A. Facchetti, and A. F. Morpurgo, J. Am. Chem. Soc., 2009, 131, 2462.
 - 2 M. Mas-Torrent and C. Rovira, Chem. Soc. Rev., 2008, 37, 827.
- 40 3 B. Kippelen and J.-L. Brédas, Energy Environ. Sci., 2009, 2, 251.
- 4 Y. Lin, Y. Li and X. Zhan, Chem. Soc. Rev., 2012, 41, 4245.
- 5 S. H. Park, A. Roy, S. Beaupre, S. Cho, N. Coates, J. S. Moon, D. Moses, M. Leclerc, K. Lee and A. J. Heeger, *Nat. Photonics*, 2009, 3, 297.
- 45 6 J. You, L. Dou, K. Yoshimura, T. Kato, K. Ohya, T. Moriarty, K. Emery, C.-C. Chen, J. Gao, G. Li and Y. Yang, *Nat. Commun.*, 2013, 4, 1446.
 - L. J. A. Koster, S. E. Shaheen and J. C. Hummelen, *Adv. Energy Mater.*, 2012, 2, 1246.
- 50 8 S. Cook, A. Furube, R. Katoh and L. Y. Han, *Chem. Phys. Lett.*, 2009, 478, 33.
- B. Verreet, B. P. Rand, D. Cheyns, A. Hadipour, T. Aernouts, P. Heremans, A. Medina, C. G. Claessens and T. Torres, *Adv. Energy Mater.*, 2011, 1, 565.
- 55 10 C. Huang, S. Barlow and S. R. Marder, J. Org. Chem., 2011, 76, 2386.
 - H. Alves, R. M. Pinto and E. S. Maçôas, *Nat. Commun.*, 2013, 4, 1842.
- M. E. Gershenson, V. Podzorov and A. F. Morpurgo, *Rev. Mod. Phys.*, 2006, **78**, 973.

- H. Najafov, B. Lee, Q. Zhou, L. C. Feldman and V. Podzorov, *Nat. Mater.*, 2010, 9, 938.
- 14 G. Hernandez-Sosa, N. E. Coates, S. Valouch and D. Moses, Adv. Funct. Mater., 2011, 21, 927.
- 65 15 N. A. Minder, S. Ono, Z. H. Chen, A. Facchetti and A. F. Morpurgo, Adv. Mater., 2012, 24, 503.
 - 16 M. Nakano, H. Alves, A. S. Molinari, S. Ono, N. Minder and A. F. Morpurgo, *Appl. Phys. Lett.*, 2010, **96**, 232102.
- 17 H. Alves, A. S. Molinari, H. X. Xie and A. F. Morpurgo, *Nat. Mater.*, 2008, **7**, 574.
- 18 M. S. Gordon and M. W. Schmidt, in *Theory and Applications of Computational Chemistry: the first forty years*, eds. C. E. Dykstra, G. Frenking, K. S. Kim and G. E. Scuseria, Elsevier, Amsterdam, 2005.
- B. Baumeier, J. Kirkpatrick and D. Andrienko, *Phys. Chem. Chem. Phys.*, 2010, **12**, 11103.
- 20 S. Cook, H. Ohkita, Y. Kim, J. J. Benson-Smith, D. D. C. Bradley and J. R. Durrant, Chem. Phys. Lett., 2007, 445, 276.
- 21 H. Wang, Y. J. He, Y. F. Li and H. M. Su, *J. Phys. Chem. A*, 2012, 116, 255
- 80 22 Y. X. Liu, M. A. Summers, S. R. Scully and M. D. McGehee, J. Appl. Phys., 2006, 99, 093521.
 - 23 P. Irkhin, A. Ryasnyanskiy, M. Koehler and I. Biaggio, Phys. Rev. B, 2012, 86, 085143.
- 24 G. Hernandez-Sosa, M. H. Tong, N. E. Coates, S. Valouch and D. Moses, *Appl. Phys. Lett.*, 2011, **99**, 163306.
- 25 J. Gao and F. A. Hegmann, Appl. Phys. Lett., 2008, 93, 223306.
- 26 I. H. Campbell and B. K. Crone, J. Appl. Phys., 2007, 101, 024502.
- A. A. Bakulin, A. Rao, V. G. Pavelyev, P. H. M. van Loosdrecht, M.
 S. Pshenichnikov, D. Niedzialek, J. Cornil, D. Beljonne and R. H.
 Friend, *Science*, 2012, 335, 1340.
- 28 G. Grancini, M. Maiuri, D. Fazzi, A. Petrozza, H. J. Egelhaaf, D. Brida, G. Cerullo and G. Lanzani, *Nat. Mater.*, 2013, 12, 29-33.
- 29 A. A. Bakulin, J. C. Hummelen, M. S. Pshenichnikov and P. H. M. van Loosdrecht, *Adv. Funct. Mater.*, 2010, **20**, 1653.
- 95 30 D. Beljonne, J. Cornil, L. Muccioli, C. Zannoni, J.-L. Brédas and F. Castet, *Chem. Mater.*, 2011, 23, 591.
 - 31 J. J. Benson-Smith, L. Goris, K. Vandewal, K. Haenen, J. V. Manca, D. Vanderzande, D. D. C. Bradley and J. Nelson, *Adv. Funct. Mater.*, 2007, 17, 451.
- 100 32 I. G. Lezama, M. Nakano, N. A. Minder, Z. H. Chen, F. V. Di Girolamo, A. Facchetti and A. F. Morpurgo, *Nat. Mater.*, 2012, 11, 788.
 - V. I. Arkhipov, P. Heremans and H. Bassler, *Appl. Phys. Lett.*, 2003, 82, 4605.